The impact of geoengineering aerosols on stratospheric temperature and ozone

2009 Environ. Res. Lett. 4 045108

(http://iopscience.iop.org/1748-9326/4/4/045108)

Environ. Res. Lett. **4** (2009) 045108 (12pp) doi:10.1088/1748-9326/4/4/045108

The impact of geoengineering aerosols on stratospheric temperature and ozone

P Heckendorn[1], D Weisenstein[2], S Fueglistaler[3], B P Luo[1], E Rozanov[1,4], M Schraner[1], L W Thomason[5] and T Peter[1]

[1] Institute for Atmospheric and Climate Science, ETH Zurich, 8092 Zurich, Switzerland
[2] AER, Lexington, MA, USA
[3] DAMTP, University of Cambridge, UK
[4] PMOD-WRC, Davos, Switzerland
[5] NASA Langley Research Center, Hampton, VA, USA

E-mail: patricia.heckendorn@env.ethz.ch

Received 29 May 2009
Accepted for publication 28 October 2009
Published 13 November 2009
Online at stacks.iop.org/ERL/4/045108

Abstract
Anthropogenic greenhouse gas emissions are warming the global climate at an unprecedented rate. Significant emission reductions will be required soon to avoid a rapid temperature rise. As a potential interim measure to avoid extreme temperature increase, it has been suggested that Earth's albedo be increased by artificially enhancing stratospheric sulfate aerosols. We use a 3D chemistry climate model, fed by aerosol size distributions from a zonal mean aerosol model, to simulate continuous injection of 1–10 Mt/a into the lower tropical stratosphere. In contrast to the case for all previous work, the particles are predicted to grow to larger sizes than are observed after volcanic eruptions. The reason is the continuous supply of sulfuric acid and hence freshly formed small aerosol particles, which enhance the formation of large aerosol particles by coagulation and, to a lesser extent, by condensation. Owing to their large size, these particles have a reduced albedo. Furthermore, their sedimentation results in a non-linear relationship between stratospheric aerosol burden and annual injection, leading to a reduction of the targeted cooling. More importantly, the sedimenting particles heat the tropical cold point tropopause and, hence, the stratospheric entry mixing ratio of H_2O increases. Therefore, geoengineering by means of sulfate aerosols is predicted to accelerate the hydroxyl catalyzed ozone destruction cycles and cause a significant depletion of the ozone layer even though future halogen concentrations will be significantly reduced.

Keywords: geoengineering, Mt Pinatubo eruption, ozone depletion, stratospheric aerosols, albedo

1. Introduction

Continuing anthropogenic greenhouse gas emissions might lead to dangerous future climate warming characterized by extreme weather events, shifting climatic zones, rising sea level and mass extinction (e.g. Hansen *et al* 2006, Solomon *et al* 2007). Considering today's political situation on this issue, doubts arise whether we will be able to reduce anthropogenic greenhouse gas emissions rapidly enough to avoid unfavourable future climatic conditions on Earth. This motivated Crutzen (2006) to suggest reconsidering the geoengineering ideas of Budyko (1977) to enhance Earth's albedo by increasing sulfate aerosol concentrations in the atmosphere. In a recent report, The Royal Society (2009) notes that such 'Solar Radiation Management techniques do not treat the root cause of climate change (increased levels of greenhouse gases in the atmosphere) but because they act quickly, they could be useful in an emergency, for example to avoid reaching a climate "tipping point" '.

During major low-latitude volcanic eruptions, significant amounts of sulfur (S) are injected into the global stratosphere. The resulting aqueous sulfuric acid aerosols reflect a portion

of the incoming shortwave (SW) radiation. The subsequent cooling of Earth's surface after volcanic eruptions has been known for a long time (e.g. Franklin 1784). The presence of enhanced aerosol loading in the stratosphere, however, not only affects the planetary albedo, but also chemical reactions and the radiative heating budget of the aerosol layer itself. For example, after volcanic eruptions, ozone depletion is observed as a consequence of accelerated heterogeneous reactions leading to depletion of active nitrogen species, and the corresponding increase in halogen catalyzed ozone destruction cycles (Solomon 1999).

Rasch *et al* (2008a) give an overview of studies addressing geoengineering by increasing Earth's albedo. Many of these studies investigated the effect of geoengineering on climate by simply reducing the incoming SW radiation (Govindasamy and Caldeira 2000, Govindasamy *et al* 2002, 2003, Matthews and Caldeira 2007, Caldeira and Wood 2008) using medium complexity General Circulation Models (GCMs). They showed that simulations of future climate with increased greenhouse gases resemble the present day climate more if geoengineering is applied.

Other model studies used stratospheric aerosol distributions similar to those observed after the Mt Pinatubo eruption as an analogue for geoengineering. Rasch *et al* (2008b) calculated equilibrium experiments with the GCM CAM3 (Community Atmosphere Model) with a slab ocean including a simplified S cycle with prescribed aerosol size distributions. They showed that the effect on surface cooling depends strongly on the size of the particles; assuming the same aerosol mass in the stratosphere for each case, small particles are more efficient scatterers of SW radiation.

Robock *et al* (2008) studied the effect of geoengineering with transient GCM simulations including an aerosol module and a coupled ocean, however, using prescribed aerosol size distributions with constant dry effective radius. They pointed out that geoengineering could lead to a reduction in precipitation, specifically the summer monsoons could be reduced. The geoengineering scenarios of Matthews and Caldeira (2007) and Rasch *et al* (2008b) also showed a decrease of precipitation in the tropical region. However, all studies suggest that the global mean climate with increased CO_2 levels is more similar to today's climate when geoengineering is applied than without geoengineering.

Tilmes *et al* (2009) analysed the effect of geoengineering on the ozone layer with a Chemistry Climate Model (CCM). They used the global model WACCM3 with a slab ocean and prescribed the aerosol loading as in Rasch *et al* (2008b). Enhanced aerosol concentrations in the stratosphere are predicted to lead to a delay of the ozone recovery of up to three decades, supporting the results of their earlier study (Tilmes *et al* 2008).

A major difference between volcanic eruptions and geoengineering-type S injections is that the latter would have to occur on a continuous basis, with important implications for the microphysical properties of the resulting aerosol. This aspect of the problem may not have received adequate attention to date. Here we use a detailed, two-dimensional microphysical aerosol model to calculate the differences in aerosol characteristics due to different S injection strategies. These results are integrated into the global CCM SOCOL to calculate the global chemical, radiative, and dynamical impacts of geoengineering.

2. Experimental setup and model description

We designed a set of equilibrium experiments with the zonal mean AER (Atmospheric and Environmental Research Inc.) 2D aerosol model (Weisenstein *et al* 1997, 1998, 2007) by injecting SO_2 into the lower tropical stratosphere. The assumption of zonally homogeneous conditions is adequate for the stratosphere, but may become more problematic in the tropical tropopause layer (Fueglistaler *et al* 2009). The aerosol model includes sulfur chemistry and all relevant microphysical processes, including nucleation, condensation, evaporation, coagulation, sedimentation and (tropospheric) washout. The aerosol size distribution is resolved by 40 size bins spanning the range 0.4 nm–3.2 μm by volume doubling. The model uses pre-calculated values of hydroxyl radical (OH) and other oxidants, along with pre-calculated photolysis rates, derived from a model calculation with standard stratospheric chemistry (Weisenstein *et al* 1997). Reaction rates are according to Sander *et al* (2000) and OH climatologies are adapted from von Kuhlmann *et al* (2003). The transport parameters in the model are prescribed as for the year 1992, the year after the eruption of Mt Pinatubo, according to the method described in Fleming *et al* (1999).

S was injected in a box centred at the equator and 20 km altitude (5°S–5°N and 19.4–20.6 km). The equator was chosen to achieve global spreading of the emitted S and resulting aerosol via the Brewer–Dobson circulation. Emissions outside the tropics would largely remain in the hemisphere of emission and have shorter residence times, as observed for mid- and high-latitude volcanoes. While the emission of engineered solid particles has been suggested to avoid particle growth by coagulation (e.g. Teller *et al* 1997, Keith 2000, Caldeira and Wood 2008) we choose S for our geoengineering simulations based on decades of observations into its behaviour in the stratosphere following volcanic eruptions. Engineered particles may have unknown and unforeseen effects, and their residence time in the atmosphere will be unknown until full-scale atmospheric experiments are conducted.

Model calculations were carried out for two types of S injection strategies: (i) continuous (with fluxes of 1, 2, 5 and 10 Mt/a S; labelled GEO1, . . . , GEO10), and (ii) pulsed with periods of 1 month (labelled GEO5p12) and 6 months (labelled GEO5p2) with fluxes of 5 Mt/a S. The mechanism for injecting S into the stratosphere is not explored in these calculations. However, a serious consideration of geoengineering operations would require that the impact of the delivery mechanism (aircraft, rockets, balloons) also be evaluated for impacts on ozone and climate.

The optical properties (using Mie theory and the refraction indices from Biermann *et al* (2000)) of the calculated aerosol are integrated into the radiative transfer calculations of the global CCM SOCOLv2.0 (SOlar Climate Ozone Links

Table 1. Geoengineering scenarios with different annual stratospheric SO_2 emissions.

Scenario	S input (Mt/a)	Special features
GEO0	0	Background S concentrations
GEO1	1	Continuous S injections
GEO2	2	Continuous S injections
GEO5	5	Continuous S injections
GEO10	10	Continuous S injections
GEO5p12	5	Monthly S injections
GEO5p2	5	Two S injections per year
GEO5_cond	5	Condensation rate/10
GEO5_coag	5	Coagulation rate/10
GEO2_24km	2	Injection altitude = 24 km
GEO2_nosed	2	No aerosol sedimentation
GEO5nC[a]	5	SAD = SAD of GEO0
GEO5nR[b]	5	Radiative effect of aerosols as in GEO0
GEO5lowODS	5	ODS concentrations of 1975
GEO5highCO2	5	Double CO_2 concentrations
GEO5lowSST	5	SI + SST climatology from 1900 to 1930

[a] In GEO5nC the heterogeneous reaction on stratospheric aerosol is as for GEO0.

[b] In GEO5nR the radiative feedback of the aerosols is set to background situation (GEO0).

Version 2.0) (Egorova *et al* 2005, Schraner *et al* 2008, Fischer *et al* 2008) and the surface area density (SAD) is integrated into the heterogeneous chemistry model part of SOCOL. The dynamical and radiative part of the model consists of the GCM MA-ECHAM4 (Middle Atmosphere version of the European Centre/Hamburg Model 4 General Circulation Model) (Manzini and McFarlane 1998), a spectral model with T30 truncation (resulting in a horizontal grid spacing of about 3.75°) with 39 levels to 0.01 hPa altitude. The chemistry is based on a modified version of the UIUC (University of Illinois at Urbana-Champaign) Chemistry Transport Model (CTM) MEZON (Model for the Evaluation of oZONe trends) (Rozanov *et al* 2001). The radiative transfer code of MA-ECHAM4 is based on the ECMWF (European Centre for Medium-Range Weather Forecast) radiation code (Fouquart and Bonnel 1980, Morcrette 1991); radiation is treated in eight spectral bands.

Twenty-year steady state experiments were performed with CCM SOCOL for the geoengineering scenarios. The boundary conditions of the CCM model runs are similar to present day conditions, with concentrations of ozone depleting substances (ODS), greenhouse gas, CO and NO_x emissions like in the year 2000 (Schraner *et al* 2008). Sea ice (SI) and sea surface temperature (SSTs) are fixed to climatological values (1994–2004) taken from the Hadley Centre HadISST data set (Rayner *et al* 2003). To study the change in surface temperature due to geoengineering, a fully interactive ocean would be required. Therefore, we focus here on stratospheric changes and changes in surface radiation. Table 1 provides a summary of all model runs used in this study; additional sensitivity calculations are described later in the text.

3. Preparatory simulations of the eruption of Mt Pinatubo

The eruption of Mt Pinatubo in June 1991 emitted 6–11 Mt S into the lower stratosphere (Guo *et al* 2004, Read *et al* 1993, McPeters 1993, Stowe *et al* 1992, Rosen *et al* 1992) and lead to a surface cooling of roughly 0.5 K one year after the eruption (Lacis and Mishchenko 1995). In the framework of the Assessment of Stratospheric Aerosol Properties (ASAP) by SPARC (Stratospheric Processes and their Role in Climate), AER model simulations have been validated with observations and other model simulations (SPARC 2006, Weisenstein *et al* 2007). The AER model ranked in this validation among the best models for stratospheric aerosols in quiescent or volcanically perturbed times. Figures 1(a)–(c) show 1 μm extinction profiles from June 1991 to December 1993 derived from LIDAR data (Antuna *et al* 2002, 2003) at Mauna Loa in Hawaii (19.54°N, 155.58°W) and Camagüey in Cuba (21.40°N, 77.92°E) and 1 μm extinction profiles of the same period calculated by the AER model at 18°N. The AER model results as calculated for the ASAP report (labelled PIN10_ASAP) show a higher peak concentration in the lower stratosphere and more aerosol at higher and lower altitudes than the observations (figures 1(a) and (b)). An AER calculation using an improved transient circulation rather than a climatology and including aerosol and gas washout up to the tropopause rather than just below 10 km is shown in figure 1(c) (labelled PIN10). Latitude–altitude profiles of backscatter ratio for May 1992 are shown in figures 1(d)–(f). Observations are from a NASA DC-8 airborne LIDAR mission during 21st, 24th, 26th of May 1992 under the coordination of Winker as a follow-on to the mission reported in Winker and Osborn (1992). Observations indicate efficient horizontal mixing within the tropical pipe but limited vertical dispersion 11 months after the eruption. PIN10_ASAP shows limited horizontal mixing and excessive vertical mixing, while the AER result with improved transport and washout (PIN10) partially corrects for this. The other models that participated in ASAP tended to produce even larger extinctions in the tropics near 30 km during the Mt Pinatubo period.

Transient SOCOL calculations from 1991 to 1999 with observed boundary conditions and AER aerosols are performed (as described in Schraner *et al* (2008), without QBO nudging). At the equator, the radiative properties calculated by SOCOL with the AER aerosols show their largest deviation from measurements in the lower stratosphere where the main aerosol cloud resided. As a consequence, the resulting heating of the lower stratosphere in the ASAP calculation was overestimated by a factor of 3–5 (green dash–dotted line PIN10_ASAP in figure 2(a)) in the first year following the eruption. By introducing the improved transient transport instead of a climatology and introducing aerosol and gas washout up to the tropopause, the performance of the AER model was improved remarkably (red dashed curve (PIN10) with 10 Mt S injection and blue solid curve (PIN7) with 7 Mt S injection in figure 2(a)). From 1993 to 1998, the AER + SOCOL results match qualitatively the ERA interim temperature analysis. Figure 2(b) shows the monthly mean,

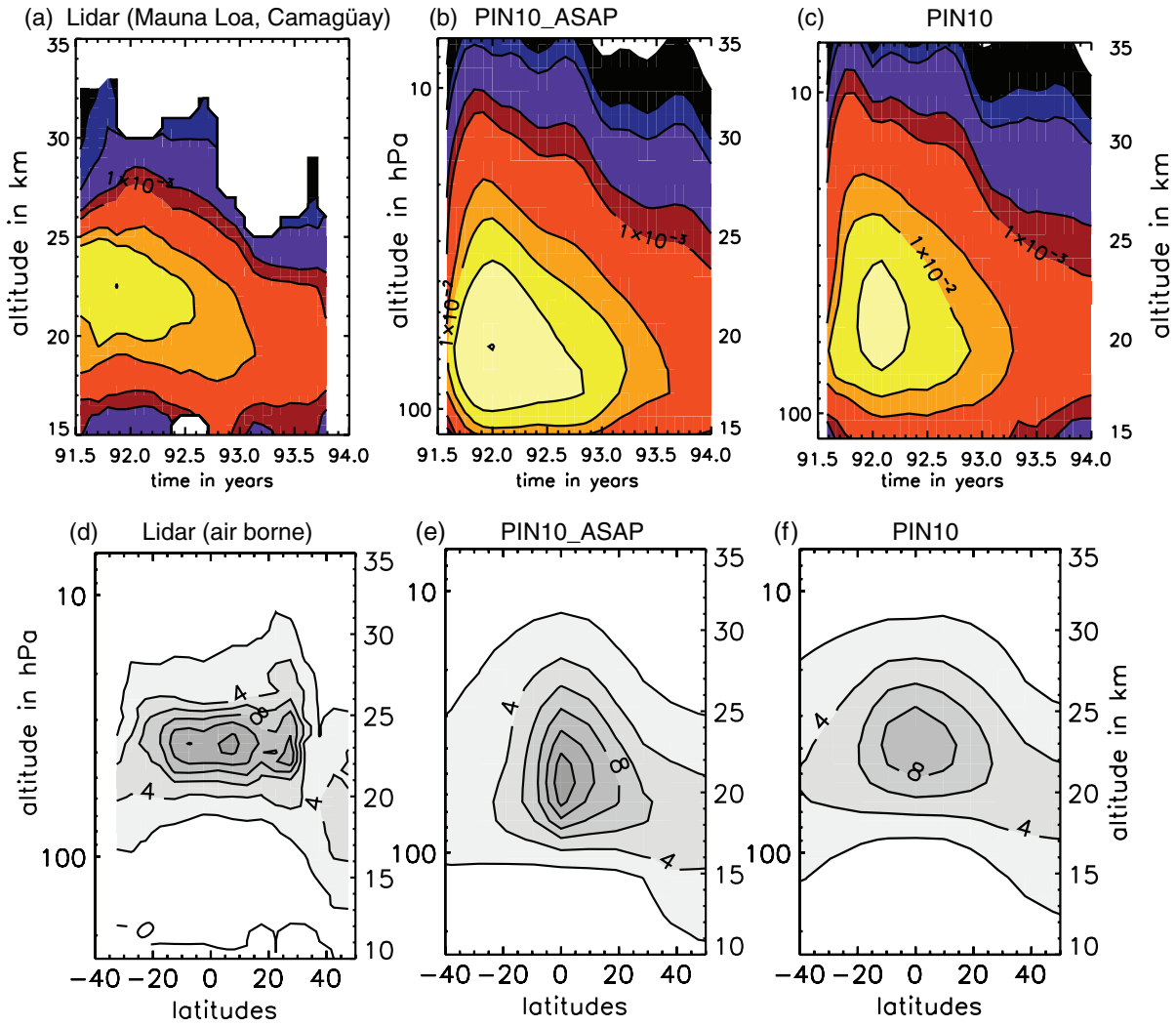

Figure 1. First row: extinction profiles from June 1991 to December 1993 at 1 μm (a) derived form LIDAR measurements at Mauna Loa and Camagüey in comparison with (b), (c) AER simulations at 18°N. Contour lines are at 1×10^{-5}, $5 \times 10^{-5} 1 \times 10^{-4}$, 5×10^{-4}, 1×10^{-3}, 5×10^{-3}, 0.01, 0.02 and 0.05 km^{-1}. Second row: backscattering ratio at 532 nm in May 1992 (d) measured by airborne LIDAR mission during 21st, 24th, 26th of May 1992 under the coordination of Winker, in comparison with (e), (f) AER model calculations (contour spacing = 2). PIN10_ASAP denotes calculations assuming 10 Mt S input as in the ASAP report (SPARC 2006), PIN10 is an improved AER calculation (see text).

zonal mean total ozone column averaged from 60°S to 60°N for observation (NIWA: New Zealand National Institute of Water and Atmospheric Research (NIWA) observational total ozone data set compiled by Bodeker *et al* (2005), TOMS: total ozone mapping spectrometer) and model calculations. PIN10_ASAP overestimates the total ozone loss, because of the overestimated surface area density (SAD). The total ozone loss due to the Mt Pinatubo eruption predicted by the CCM SOCOL using the improved AER simulations (PIN10, PIN7) is in the same range as observed by NIWA and TOMS.

4. Geoengineering aerosol particle distributions

The total S loading and the particle size are the key variables for the radiative and chemical impact of the aerosols from geoengineering. Particles with radii in the range of 0.1 μm are most efficient in cooling the Earth's surface, as these particles have the largest backscattering cross section per unit mass. The number density and the size distribution of the aerosol defines the surface area density (SAD) which is crucial for the changes in chemistry. Figure 3 shows the SAD of the sulfuric acid aerosols formed after the injection of 1–10 Mt/a S calculated by the AER aerosol model. The largest values of SAD and hence the largest concentration of stratospheric aerosols is in the tropical region. The more S is continuously emitted, the larger the SAD gets. GEO5 shows SAD larger than 40 μm^2 cm^{-3} near the injection region (20 km, equator, figure 3(d)). If the S injection takes place only twice a year (GEO5p2), the annual mean SAD in the injection region gets larger than 100 μm^2 cm^{-3} (figure 3(f)). Below the injection region, the SAD is strongly enhanced due to geoengineering, indicating the importance of sedimentation of the particles to lower altitudes.

Figure 4(a) shows the annual global mean aerosol loading (in Mt S) for the different scenarios when steady state is reached. The dash–dotted line in the figure represents the

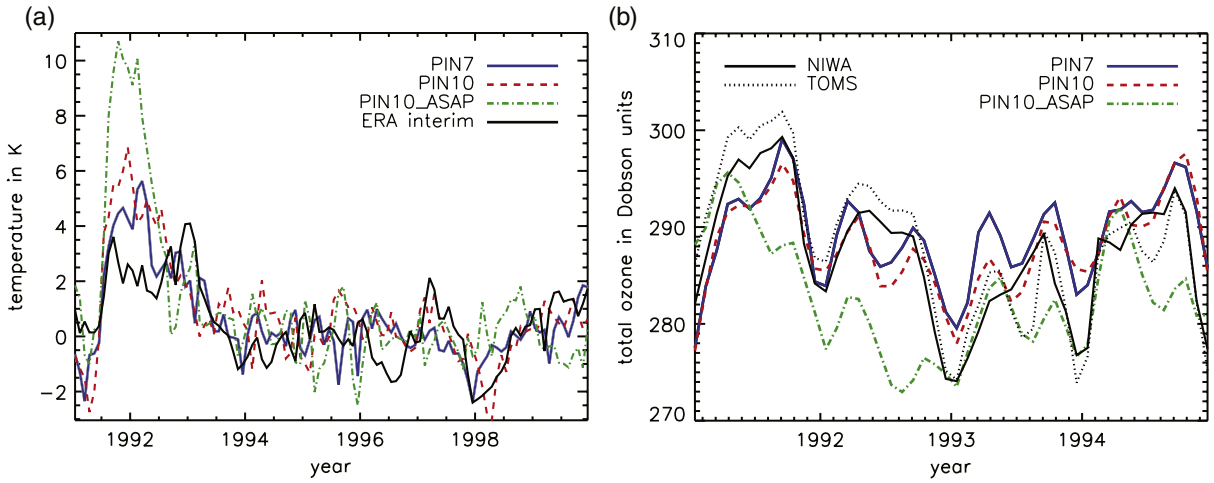

Figure 2. (a) Zonal mean monthly mean temperature difference at 50 hPa in the tropics (20°S–20°N) relative to zonal mean monthly mean temperature averaged over 1996–1999 for the same region. (b) Zonal mean monthly mean total ozone column average from 60°S to 60°N from January 1991 to December 1994.

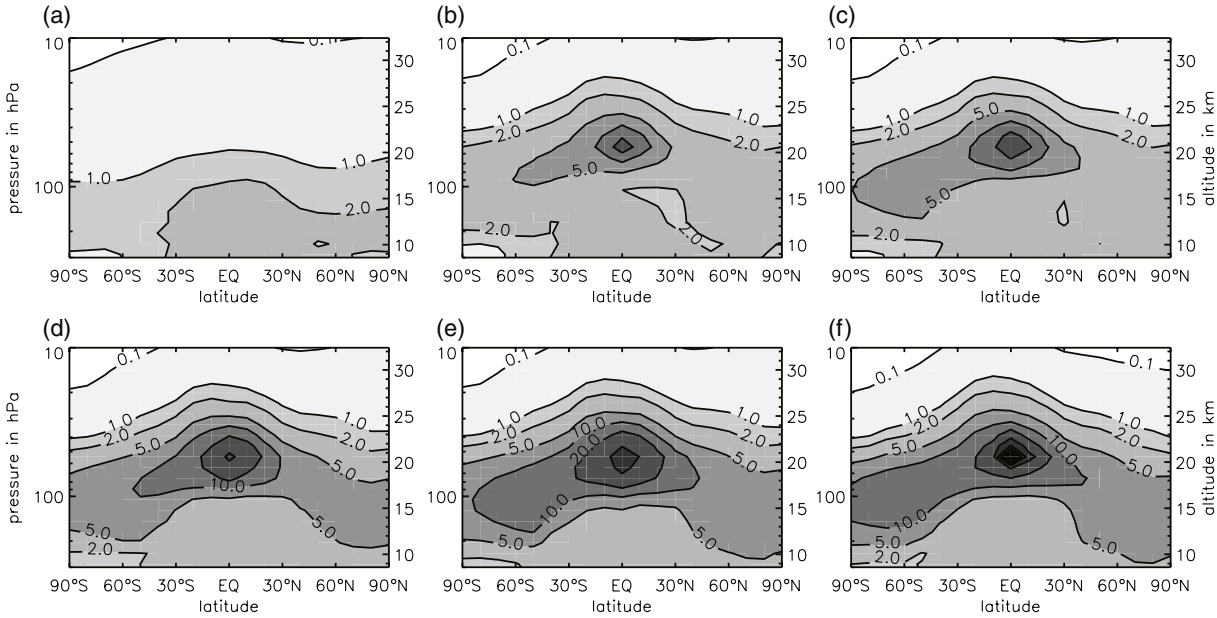

Figure 3. Annual mean zonal mean surface area density in μm^2 cm^{-3} of base run (a) (GEO0) and geoengineering scenarios (b)–(e), (f) (GEO1–GEO10, GEO5p2) in the vertical range from 300 to 10 hPa. Contour lines are at 0.1, 1, 2, 5, 10, 20, 50, 100 μm^2 cm^{-3}.

aerosol burden that would be expected if the stratospheric residence time were one year in all cases, which was observed for the 1992–1993 period immediately following the Mt Pinatubo eruption (McCormick *et al* 1995). We find that smaller (larger) particles have a longer (shorter) residence time. For 1 Mt/a S emission (GEO1), the equilibrium aerosol burden in the atmosphere is 1.4 Mt S, slightly above the line. For all other simulations the stratospheric residence time of the aerosol is shorter than one year: the aerosol burden for GEO2 is 2.1 Mt S, for GEO5 3.7 Mt S and for GEO10 6.0 Mt S. If the S emission occurs at higher altitude, the residence time of the aerosol increases; the annual emission of 2 Mt/a (5 Mt/a) S at 24 km yields a mean aerosol burden of 2.5 Mt S (4.6 Mt S).

These results are very different from those of Rasch *et al* (2008b) (and consequently also Tilmes *et al* 2009), who calculate an S loading of 5.9 Mt S for 2 Mt/a S injected at 24 km for an aerosol distribution with fixed effective radius of 0.43 μm. In our calculations, aerosol particles grow sufficiently large to allow gravitational settling to become an important sink. If aerosol sedimentation is turned off in the model (GEO2_nosed), the aerosol burden increases to 7.8 Mt S. These dramatic differences in calculated aerosol loading require thorough analysis, as they have a large impact on the consequences of geoengineering.

After volcanic eruptions, the mode radius of the aerosol size distribution is typically in the range of 0.3–0.5 μm, roughly 5–8 times larger than during quiescent times (e.g. Steele and Hamill 1983, Thomason 1992, Deshler *et al* 1992). Crutzen (2006) and Robock *et al* (2008) assumed that the effective radius would be rather smaller for geoengineering

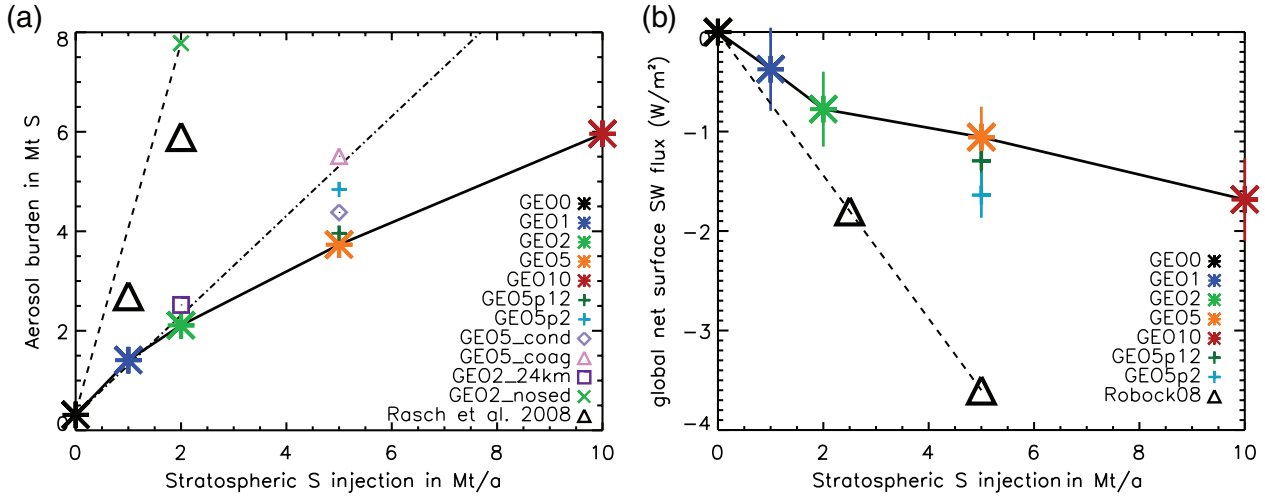

Figure 4. (a) Total aerosol burden as function of sulfur injected annually into the stratosphere (0, 1, 2, 5 and 10 Mt/a S) calculated by the AER model. Dash–dotted line: aerosol burden, if the aerosol residence time were 1 year irrespective of injection strength. Dashed line: aerosol burden when aerosol sedimentation is suppressed in the stratosphere. All results for injections at 20 km, except black square for 24 km emissions. (b) Change in global annual mean net SW flux change at the surface due to geoengineering in comparison with GEO0 calculated by SOCOL for all-sky conditions. Vertical bars: standard deviation of monthly values. Triangles: SW downward flux changes due to geoengineering as proposed by Robock *et al* (2008). All lines in both panels are meant to guide the eye.

than for the Mt Pinatubo eruption, due to a continuous supply of S and the resulting 'reduction of coagulation'. The AER model results show, in contrast, depending on the S loading, that the geoengineering aerosols could grow larger than particles formed after the Mt Pinatubo eruption. Figure 5 shows the aerosol size distribution (in differential number density) in the equatorial stratosphere for different AER simulations. In the lower stratosphere, the mode radius increases with increasing amounts of S emission from 0.1 to 0.6 μm when going from GEO1 to GEO10 (figures 5(a)–(c)). At the equator and 55 hPa altitude, the annual mean aerosol loading of GEO5 is comparable to the mean aerosol loading the first year of the Mt Pinatubo simulation (PIN10), however, GEO5 produces larger mode radii than PIN10 (figure 5(e)).

Aerosol growth depends on competition between nucleation, condensation and coagulation. The freshly formed H_2SO_4 molecules either stay in the gas phase, nucleate together with H_2O molecules to form stable clusters, or condense on pre-existing aerosols. In the injection region, the gas-to-particle flux by condensation is 4–6 orders of magnitudes larger than the flux by nucleation. The growth of the large particles ($r > 1$ μm) is either due to condensation or to coagulation. We performed sensitivity tests with reduced condensation and coagulation rates to test the importance of these two processes (table 1). If the coagulation rate is reduced by a factor 10 (GEO5_coag), the mode radius is reduced by roughly a factor of 2 (figures 5(g)–(i)). Consequently the gravitation loss of the aerosol is reduced, and with the same annual S input, GEO5_coag has a 46% larger aerosol burden than GEO5 (figure 4(a)). In scenario GEO5_cond the condensation rate is reduced by a factor 10, which leads to a shift in importance of the gas-to-particle flux from condensation towards nucleation. Hence, more tiny particles are formed which grow by coagulation. The mode radius of the GEO5_cond size distribution (with reduced condensation rate by a factor 10) is smaller than the mode radius of GEO5 (see figures 5(g)–(i)) and consequently the gravitational loss is reduced by 17%.

The geoengineering scenarios with continuous S supply lead to a continuous supply of H_2SO_4, and therefore continuous particle growth by condensation. But even more important for the growth of large particles is the continuous supply of freshly nucleated small particles ($r < 0.03$ μm) which coagulate rapidly with larger particles, leading to even larger particles ($r > 0.4$ μm). In contrast to the volcanic case where coagulation is self-limited by number densities that decrease with time, the abundance of small particles is never depleted under geoengineering emissions. Thus coagulation is the most important process in the formation of large particles ($r > 1$ μm) in our calculations. Because gravitational fall speed scales with the square of the particle radius, the formation of large particles strongly increases gravitational removal of the aerosol and decreases its residence time relative to the volcanic case.

The temporal and spatial distribution of S injection has a strong influence on the particle size distribution. In our experiments the S is distributed over a zonal band of 9.5° wide and 1.2 km high. To test the dependence of particle growth on the spatial distribution we performed three more geoengineering calculations with the source of 5 MT/a S: in the first experiment the SO_2 is injected at the equator as well but spread vertically from 20 to 25 km, the second spread emissions from 30°S to 30°N, with emissions at 20 km only and the third spread emissions in the same latitudinal range as the second but additionally spread emissions vertical from 20 to 25 km. The first produced a burden of 4.5 Mt S, the second a burden of 4.3 Mt S, the third a burden of 4.8 Mt S. Thus the spreading of emissions is one potential method to improve the efficiency of geoengineering injections, though the

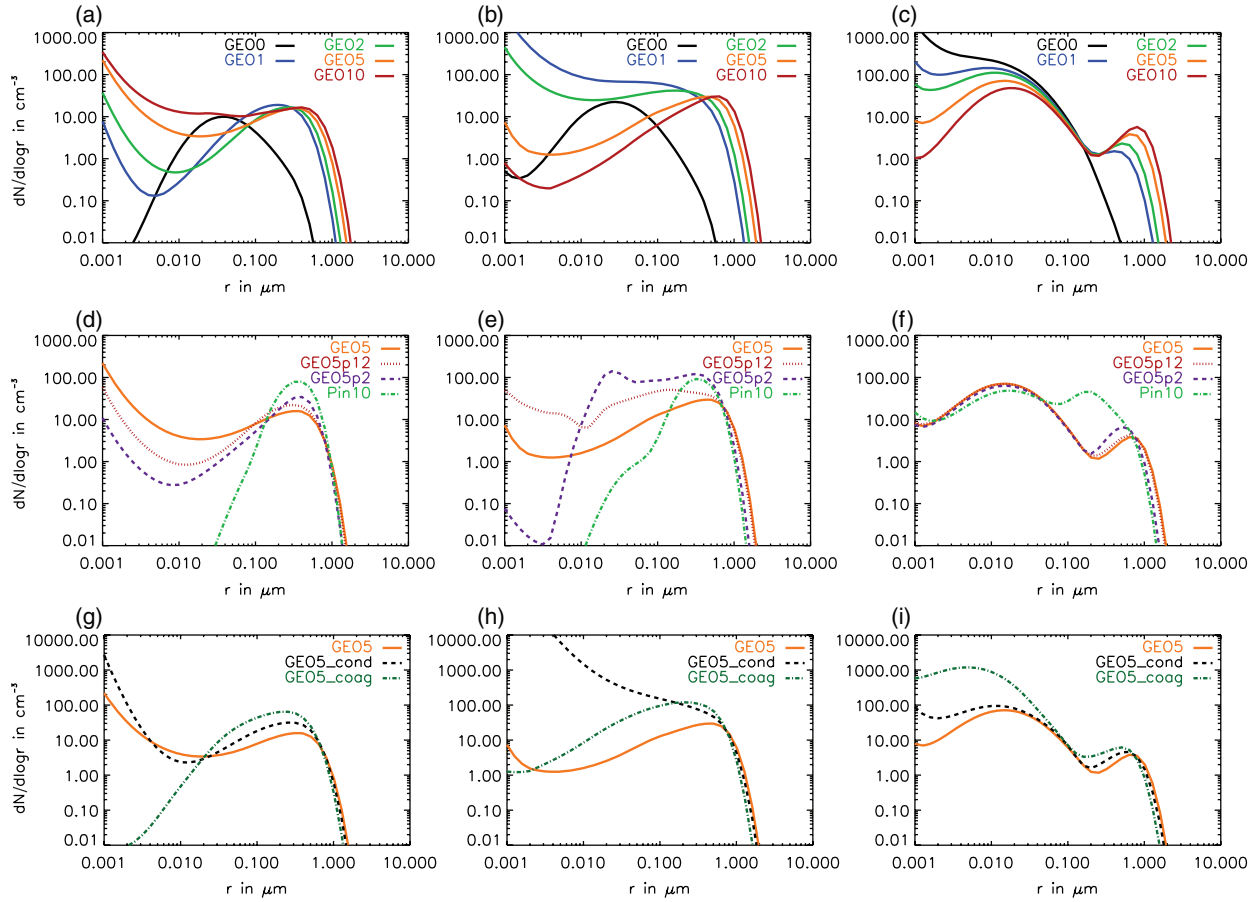

Figure 5. Annual mean differential number density $\mathrm{d}N/\mathrm{d}\log r$ in cm^{-3} at the equator at 39 hPa (first column), 55 hPa (second column) and 90 hPa (third column). (a)–(c) Continuous S injection into the lower stratosphere of 0, 1, 2, 5 and 10 Mt/a (GEO0–GEO10). (d)–(f) Continuous and pulsed emission of 5 Mt/a S emissions (GEO5, GEO5p12, GEO5p2) and annual mean aerosol size distribution for PIN10 from June 1991 to May 1992. (g)–(i) GEO5, GEO5_cond with reduced condensation rates and GEO5_coag with reduced coagulation rates.

continuous nature of the emission still leads to particles larger than expected based on volcanic analogues.

As shown above, the constant supply of H_2SO_4 and the subsequent supply of small aerosols leads to the formation of large particles. Pulsed emissions of SO_2, in contrast, help to reduce the mode radius of the aerosol distribution. A monthly injection (GEO5p12) reduces the mode radius slightly (figures 5(d)–(f)), and consequently less S is lost by gravitational settling (6% larger aerosol loading than GEO5, figure 4(a)). If SO_2 is only emitted twice a year (GEO5p2), the mode radius could be reduced by up to 50% and the equilibrium aerosol loading increased by 30%. As the particles in GEO5p2 are much smaller than in GEO10, GEO5p2 has a much higher SAD in the injection region than GEO10 (figure 3).

5. Changes in the stratosphere

When assuming present day halogen concentrations, all of the geoengineering scenarios listed in table 1 lead to reductions in the total O_3 column. Figure 6 shows the change in annual mean zonal mean total O_3 column as a function of latitude; the global mean values are listed on the plots. For GEO5 (GEO10) the annual mean global mean total O_3 column is predicted to decrease by 4.5% (5.3%) in comparison to GEO0. This is more than the annual mean global mean total O_3 loss due to the emission of anthropogenic ODS, which was −3.5% averaged from 2002 to 2005 in comparison to the 1964–1980 average as determined from observations (WMO 2007, chapter 3) or −3.8% calculated by SOCOL (for nine members in an ensemble calculation) averaged from 1996 to 1999 in comparison to the 1964–1980 average (Fischer *et al* 2008). In the same period the observed tropical O_3 loss was negligible, but for the geoengineering scenarios the tropical O_3 loss is remarkable: in GEO5 (GEO10) the annual tropical mean total O_3 column (25°S–25°N) is reduced by 3.5% (4.3%).

On the sulfate aerosols the N_2O_5 hydrolysis leads to the formation of the stable reservoir species HNO_3:

$$N_2O_5(\mathrm{g}) + H_2O(\mathrm{l,\,s}) \xrightarrow{\mathrm{HET}} 2HNO_3(\mathrm{s}). \qquad (1)$$

This leads to a lowering in the NO_x/NO_y ratio. Hence the NO_x catalyzed O_3 destruction cycles become less important and the formation of the reservoir gas $ClONO_2$ is reduced, yielding an increase in the ClO_x/Cl_y ratio. At the same time chlorine is

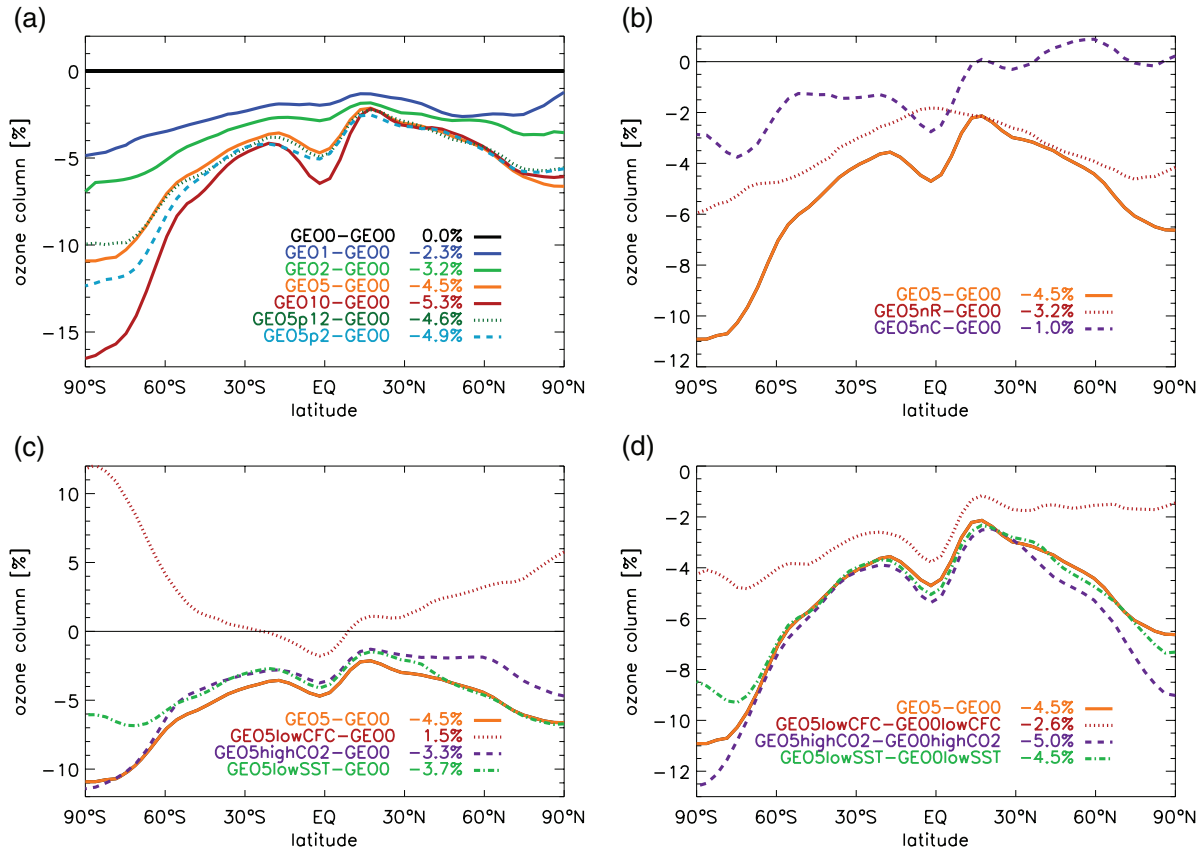

Figure 6. Predicted geoengineering-induced changes in annual mean zonal mean total ozone column. Listed values show annual global mean values. (a) Standard scenarios (solid curves) and pulsed scenarios (dotted: monthly; dashed: semiannually) relative to GEO0. (b) Scenarios with no surface enhancement (nC) and no radiative enhancement (nR) relative to GEO0. (c) Special scenarios with low CFC, high CO_2 or low SST relative to GEO0. (d) Same as in (c), but relative to special scenarios without geoengineering. The orange GEO5–GEO0 curve is shown in all panels for clarity.

further activated due to the heterogeneous reaction:

$$\mathrm{ClONO_2(g) + HCl(s) \xrightarrow{HET} Cl_2(g) + HNO_3(s).} \qquad (2)$$

These processes enhance ClO_x-induced ozone destruction. Ozone destruction by bromine is enhanced through similar mechanisms, but to a much smaller extent.

Figure 7 shows the vertical profiles of the zonal mean O_3 changes due to geoengineering for the south polar region (a), for the tropics (b) and for the north polar region (c). Figure 8 shows the change in O_3 destruction rates (in percentage) due to the injection of 5 Mt/a S (GEO5–GEO0) for different destruction cycles. In the middle stratosphere the most dominant O_3 destruction cycle is catalyzed by NO_x. The slowing of this cycle due to geoengineering leads to less O_3 destruction, hence an increase in the tropical mean O_3 concentration between 30 and 35 km (figures 7(b) and 8(b)). In the lowermost stratosphere the halogen and HO_x catalyzed destruction cycles are more important, hence the increased ClO_x and BrO_x concentrations lead to O_3 destruction in this region. In the polar spring region the O_3 depletion is enhanced especially in the lowermost stratosphere (200–80 hPa) (figures 7(a) and (c)). This corresponds about to the observed O_3 loss in the polar spring regions after Mt Pinatubo eruption (e.g. Deshler *et al* 1994, 1992, Hofmann and Oltmans 1993).

5.1. Heating of the lower stratosphere and increase of stratospheric water vapour

Another feedback on stratospheric O_3, which has not been discussed previously, is caused by the heating of the tropical tropopause region and the subsequent increase of stratospheric water vapour (H_2O). All AER scenarios show an increased level of stratospheric aerosols near the tropical tropopause due to injection of SO_2 at 20 km. This results in heating of the tropical tropopause region, mainly due to absorption of longwave (LW) radiation. The more sulfate aerosol is present in the tropical tropopause region, the larger is the resulting heating; this relationship is shown in figure 9. The temperature at 90 hPa at the equator is 2.8 K higher in GEO10 than in the base run (GEO0). In GEO5 the temperature near the tropopause rises by 1.3 K. With the same optical aerosol properties, but SADs equal to background concentrations (GEO5nC), the temperature increase would be 0.4 K larger than for GEO5, because in scenario GEO5 the O_3 decrease, due to enhanced heterogeneous reactions, cools the tropical tropopause. Therefore the cold point temperature for GEO5nR is 0.3 K lower than for the base run. As the stratospheric

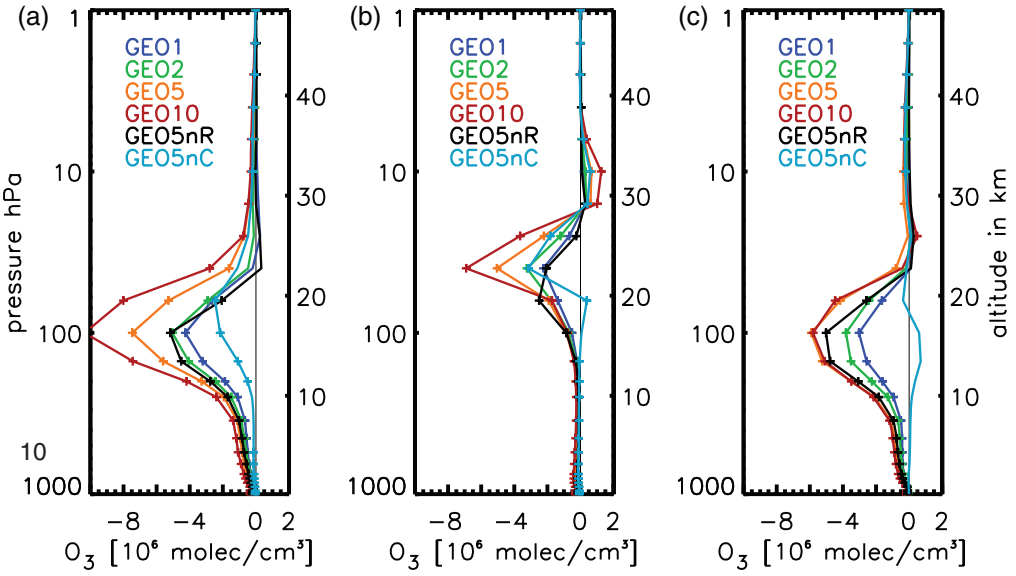

Figure 7. Annual zonal mean O_3 (in 10^6 molecules cm^{-3}) changes with respect to GEO0 (a) in the south polar region (60°S–90°S), (b) in the tropics (30°S–30°N), (c) in the north polar region (60°N–90°N). Plus signs indicate changes to be statistically significant on the 95%-confidence interval (*t*-test).

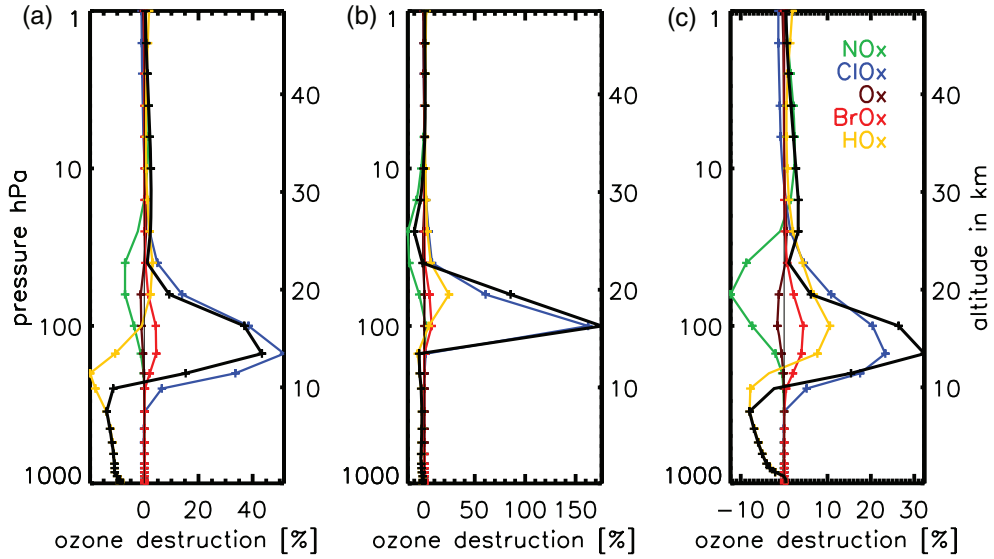

Figure 8. Change in annual zonal mean ozone destruction rate due to injection of 5 Mt/a S (GEO5) in the lower stratosphere. (a) Southern high latitudes (60°S–90°S), (b) tropics (30°S–30°N), (c) northern high latitudes (60°N–90°N). Change of loss rate in per cent relative to the total chemical destruction rate (sum of all destruction cycles) of base run GEO0. Black curve: change in total chemical ozone destruction. Coloured lines: nitrogen (NO_x), chlorine (ClO_x), hydrogen (HO_x), bromine (BrO_x) catalyzed destruction cycles and cannibalistic reactions (O_x). The BrO_x catalyzed destruction includes the destruction by the coupled BrO_x–ClO_x-destruction cycle. Plus signs indicate statistically significant changes on the 95%-confidence interval (*t*-test).

H_2O concentration depends on the minimum temperature in the profile, the annual mean H_2O concentrations interpolated at 90 hPa are smaller than the corresponding temperatures at this altitude would suggest (Fueglistaler *et al* 2005). The non-linear warming of the tropical tropopause with increasing S injection leads consequently to a non-linear increase of stratospheric H_2O. For GEO5, H_2O concentrations at 90 hPa increase by 0.7 ppmv and for GEO10 by 1.6 ppmv.

As a consequence, the HO_x catalyzed O_3 destruction cycles are intensified, which leads to a decrease in O_3 in the upper and lower stratosphere (figure 8(b)). GEO5nR (with slightly decreasing stratospheric H_2O concentrations) shows a small increase in O_3 above 38 km. Additionally the increased stratospheric H_2O intensifies the formation of HNO_3 and decreases further the NO_x/NO_y ratio. Therefore, even without increased N_2O_5 hydrolysis (GEO5nC), O_3 concentrations in the tropical middle stratosphere increase. In the tropical area, three fifths of the total O_3 loss can be attributed to the stratospheric warming and subsequent increase of stratospheric H_2O (GEO5nC), whereas two fifths is attributed to enhanced heterogeneous reactions on sulfate aerosols and a shift in ClO_x/Cl_y ratio (GEO5nR).

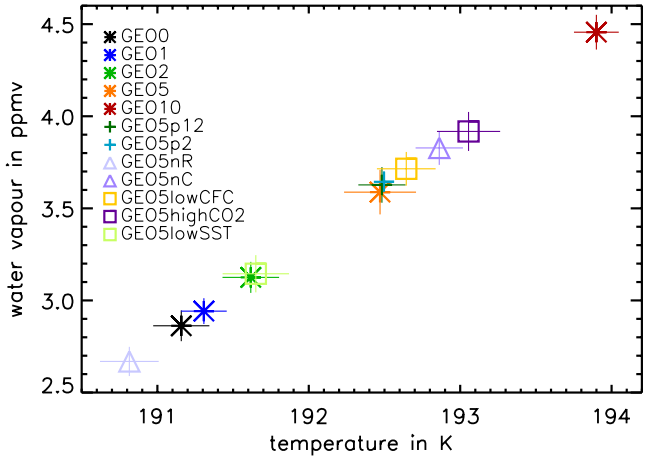

Figure 9. Annual mean water vapour in relation to annual mean temperature, both at 90 hPa at the equator, i.e. close to the tropical tropopause. The slope of this relationship is in good agreement with the Clausius–Clapeyron equation of water vapour pressure over ice.

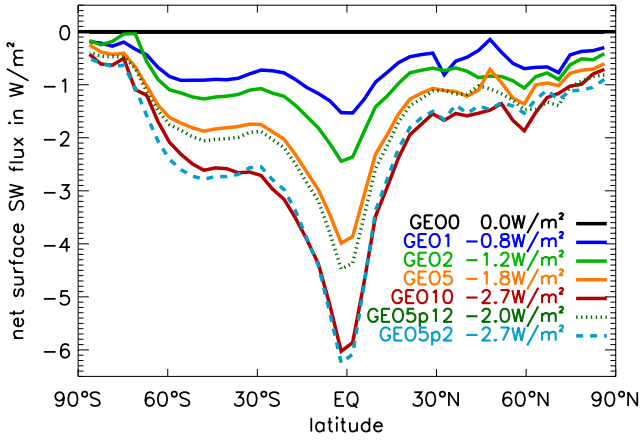

Figure 10. Change in zonal mean annual mean net SW flux at the surface in W m^{-2} due to geoengineering for clear-sky conditions with respect to the base run (GEO0). Listed values show change in annual mean global mean SW flux.

The increased meridional temperature gradient in the stratosphere tends to intensify the polar vortex. The resulting cooling of the polar region and the higher stratospheric H_2O concentrations enhance PSC formation (statistical significant increase on the 95% confidence interval of up to 100%). Therefore the O_3 in the polar spring region is additionally depleted due to enhanced ClO_x and BrO_x catalyzed ozone destruction cycles (figures 7(a), (c) and 8(a), (c)).

5.2. Sensitivity of O_3 loss to future halogen and CO_2 concentrations and SSTs

In the future, halogen concentration will decrease and therefore O_3 destruction will be reduced. The sensitivity run GEO5lowCFC has the same boundary conditions as GEO5 except for lower halogen concentrations (as in 1975). The global total ozone column of GEO5lowCFC is 1.5% higher than of GEO0, but compared to low halogen concentrations without geoengineering (GEO0lowCFC) the global total ozone column would still decrease by 2.6% (figures 6(c) and (d)). In contrast to the finding of Tilmes *et al* (2009), that the tropical total ozone layer will increase with geoengineering and lower CFCs, we find that due to the strong warming of the lower stratosphere (and the following moistening of the stratosphere) the tropical total ozone column is predicted to decrease, even with future low halogen concentrations.

To test the sensitivity of stratospheric changes due to geoengineering to changes in SST we performed a run with SST and SI climatology from 1900 to 1930 (GEO5lowSST). With lower SSTs, the cold point temperature is lower and therefore the stratosphere is dryer than in GEO5 (figure 9). As a consequence, less O_3 is destroyed by HO_x destruction cycles and the global total ozone column is higher than for GEO5.

In the future the CO_2 concentration will increase. GEO5highCO2 is a geoengineering scenario like GEO5 but with doubled CO_2 concentrations. In our experiment GEO5highCO2 has a higher temperature at the tropical tropopause and leads to a wetter stratosphere. Therefore in a doubled CO_2 world the total O_3 depletion would be larger when geoengineering is applied (figure 6(d)).

Table 2. Change in global mean annual mean net SW flux at the surface plus/minus standard deviation due to geoengineering in comparison with GEO0. Calculated by SOCOL for clear-sky and all-sky conditions.

Scenario	Clear-sky SW Flux change (W m^{-2})	All-sky SW Flux change (W m^{-2})
GEO1	-0.78 ± 0.10	-0.37 ± 0.42
GEO2	-1.16 ± 0.11	-0.78 ± 0.38
GEO5	-1.81 ± 0.09	-1.06 ± 0.31
GEO10	-2.67 ± 0.11	-1.68 ± 0.42
GEO5p12	-2.00 ± 0.08	-1.29 ± 0.35
GEO5p2	-2.66 ± 0.08	-1.64 ± 0.23
Robock08[a] (2.5 Mt/a)		-1.8
Robock08[a] (5 Mt/a)		-3.6

[a] Additionally listed are SW downward flux changes due to geoengineering as proposed by Robock *et al* (2008).

6. Changes in surface radiation by geoengineering

Figure 10 shows changes in annual mean zonal mean surface net clear-sky SW flux (with wavelength of 0.25–4 μm) calculated by SOCOL for the different geoengineering scenarios. The largest changes occur in the tropics, as the largest part of the aerosol mass is located in this region. The global mean clear-sky SW flux of GEO2 is 1.2 W m^{-2} lower than of GEO0 (table 2), which is in the same range as today's radiative forcing due to direct and indirect aerosol effects (Forster *et al* 2007). GEO5 (GEO10) leads to a change in global mean clear-sky SW flux of -1.8 W m^{-2} (-2.7 W m^{-2}). In the presence of clouds the SW flux change (all-sky) is smaller than for clear-sky condition. In figure 4(b) the change in global annual mean SW flux as a function of injected S is shown (see also table 2). Both the non-linear loss by gravitational settling with increasing S loading and the distribution of condensed mass on larger particles cause the SW flux to grow non-linearly with S injections.

GEO5p2 has a 20% smaller S loading than GEO10, but as GEO5p2 contains much more small particles (which more efficiently scatter SW radiation) the surface SW flux change of GEO5p2 and GEO10 are almost equal. GEO10 shows a net all-sky SW flux change of 1.7 ± 0.4 W m^{-2} compared to GEO0. This flux is approximately equal to the radiative forcing introduced by geoengineering (when changes in the LW budget are neglected). The estimates of the climate sensitivity (defined as the equilibrium temperature response following the doubling of CO_2) range between 2 and 4.5 K with the most likely value of 3 K (Hegerl *et al* 2007). Assuming that CO_2 doubling leads to a forcing of 3.8 W m^{-2} (Meehl *et al* 2007), the climate sensitivity parameter (defined as the fraction of the temperature change and applied forcing (dT/dF)) is 0.5–1.2 K/(W m^{-2}) with the most likely value of 0.8 K/(W m^{-2}). Hence the global mean temperature due to GEO10 would decrease by $-$(0.7–2.5 K) with the most likely value of -1.4 K.

Robock *et al* (2008) calculated a linear increase in SW flux change with increasing S injections: according to their simulation a 2.5 Mt/a S injection yields a global reduction of downward SW radiation at the surface of -1.8 W m^{-2}. They assume an effective radius of 0.30–0.35 μm (which is most probably underestimated) and therefore the gravitational loss is very small.

Changes in stratospheric H_2O and O_3 also influence the temperature change at the surface. With increasing S injections, stratospheric H_2O increases, leading to an increased positive LW radiative forcing at the surface. The stratospheric H_2O in GEO10 increases by roughly 1.5 ppmv (figure 9). Forster and Shine (2002) showed that an increase of 1 ppmv H_2O above 10 hPa leads to RF of 0.3 W m^{-2}, which means that the cooling achieved by the increased albedo might be reduced significantly. However, the loss in stratospheric O_3 at the same time decreases the greenhouse gas forcing. Detailed radiative forcing calculation are beyond the scope of this letter and should be addressed in the future.

7. Discussion and conclusions

The 2D AER aerosol model was used to simulate geoengineering scenarios where global albedo is reduced with the help of stratospheric sulfuric acid aerosol enhancements. The AER model resolves all relevant microphysical processes in the formation of sulfuric acid aerosols after injection of SO_2 into the stratosphere. In a model–observation comparison by SPARC (2006), the AER model ranked among the best models for the description of the stratospheric aerosol formation after volcanic eruptions. As already mentioned above, in the tropical tropopause layer (TTL) zonally inhomogenic processes (as for instance washout by convective systems) could become important and then the zonal mean model might be problematic. In the tropics, where the uncertainties in the aerosol observation after the Mt Pinatubo eruption are largest, the model overestimates the extinction by the aerosol. This could be caused by deficiencies in the microphysics or by too slow transport of the aerosol to higher latitudes. However, the clear distinction that the model allows to draw between the various geoengineering scenarios and unperturbed conditions suggests that the conclusions reached in this letter are robust.

We performed hypothetical geoengineering experiments where S in the form of SO_2 is continuously emitted at the equator at 20 km altitude. The continuous emission of S leads to aerosol size distributions with larger mode radii than observed and modelled after volcanic eruptions. Continuous coagulation of the freshly nucleated geoengineering particles with the already grown background particles is identified to be the most important process for the formation of large particles, and condensation further adds to the aerosol growth. The geoengineering particles grow to such sizes that they experience substantial gravitational settling and have accordingly shorter residence times in the stratosphere. This results in a non-linear relationship between stratospheric sulfate aerosol burden and SO_2 emission. Another drawback of the formation of large aerosols is the reduced SW scattering efficiency with increasing size of the particles. Hence larger amounts of S would be needed in order to counteract global warming.

The continuous emission of S in the tropical lower stratosphere could lead to a heating of the tropical tropopause region. According to our model simulations, the tropical cold point temperature increases by half (one) a degree due to the emission of 5 Mt/a S (10 Mt/a S). A warming of this sensitive region induces a moistening of the stratosphere. As a caveat, analyses of the Mt Pinatubo eruption show that the lower stratospheric warming is possibly overestimated by our model. However, many CCMs presently suffer from this problem, see Eyring *et al* (2006). This suggests that current models have a problem which may not yet have received the attention it deserves.

If the S would be deposited only twice per year instead of continuously, the mode radius of the aerosol size distribution would be smaller and hence less S would be lost. However, the injection of such large amounts of S in a short time would be unfavourable from a technical point of view. Spreading the emissions over a larger area is another strategy to reduce the particle size and improve the efficiency of geoengineering by S injection. Furthermore, use of particles other than sulfate to reduce the global SW surface flux could perhaps avoid some of the drawbacks and side-effects presented here, provided these particles could escape coagulation, but additional unknowns would then need to be investigated.

For present-day halogen concentrations, the stratospheric O_3 is depleted in our geoengineering scenarios, with most intense loss in the tropical and polar regions. The global mean total O_3 column is depleted by 4.5% due to the emission of 5 Mt/a S. Three quarter of the increase in global total O_3 loss could be attributed to heterogeneous reactions, resulting in a shift in the NO_x/NO_y ratio and in halogen activation. One quarter could be attributed to the increase of temperature in the lower stratosphere and the moistening due to increased tropical cold point temperature. In the tropics, heterogeneous reactions cause a smaller fraction ($\sim$40%) of the O_3 loss than the heating of the lower stratosphere ($\sim$60%). Experiments with reduced halogen concentration (as in 1979) suggest O_3 loss in the tropics is caused by temperature increase and moistening of the stratosphere. Another drawback of the potential moistening of the stratosphere due to geoengineering is the additional positive LW forcing, which reduces the surface cooling.

Acknowledgments

PK is funded by ETH Zurich (S-ENETH project TUMSS), DW by NASA ACMAP program, BPL by the EU project SCOUT-O3, MS and ER by the ETH Zurich Polyproject 'Variability of the Sun and Global Climate Phase I + II'. We would like to thank Andreas Fischer, Stefan Broennimann, Marco Giorgetta, Gera Stenchikov, Manu Thomas, Claudia Timmreck, Simone Tilmes and Sebastian Schmidt for helpful discussions.

References

Antuna J C, Robock A, Stenchikov G L, Thomason L W and Barnes J E 2002 *J. Geophys. Res. Atmos.* **107** 4194
Antuna J C, Robock A, Stenchikov G, Zhou J, David C, Barnes J and Thomason L 2003 *J. Geophys. Res. Atmos.* **108** 4624
Biermann U M, Luo B P and Peter T 2000 *J. Phys. Chem.* A **104** 783–93
Bodeker G E, Shiona H and Eskes H 2005 *Atmos. Chem. Phys.* **5** 2603–15
Budyko M I 1977 *Tellus* **29** 193–204
Caldeira K and Wood L 2008 *Phil. Trans. R. Soc.* A **366** 4039–56
Crutzen P J 2006 *Clim. Change* **77** 211–9
Deshler T, Adriani A, Gobbi G P, Hofmann D J, Didonfrancesco G and Johnson B J 1992 *Geophys. Res. Lett.* **19** 1819–22
Deshler T, Hoffman D J, Johnson B J and Rozier W 1992 *Geophys. Res. Lett.* **19** 199–202
Deshler T, Johnson B J and Rozier W 1994 *Geophys. Res. Lett.* **21** 273–6
Egorova T A, Rozanov E V, Zubov V N, Manzini E, Schmutz W and Peter T 2005 *Atmos. Chem. Phys.* **5** 1557–76
Eyring V *et al* 2006 *J. Geophys. Res. Atmos.* **111** D22308
Fischer A *et al* 2008 *Atmos. Chem. Phys.* **8** 7755–77
Fleming E, Jackman C, Stolarski R and Considine D 1999 *J. Geophys. Res. Atmos.* **104** 23911–34
Forster P and Shine K 2002 *Geophys. Res. Lett.* **29** 1086
Forster P *et al* 2007 *Climate Change 2007: The Physical Science Basis. Contribution of Working Group I to the Fourth Assessment Report of the Intergovernmental Panel on Climate Change* ed S Solomon, D Qin, M Manning, Z Chen, M Marquis, K B Averyt, M Tignor and H L Miller (Cambridge: Cambridge University Press)
Fouquart Y and Bonnel B 1980 *Contrib. Atmos. Phys* **53** 35–62
Franklin B 1784 *Manchester Literary and Philosophical Society Memoirs and Proc.* vol 2, p 122
Fueglistaler S, Bonazzola M, Haynes P H and Peter T 2005 *J. Geophys. Res.* **110** D08107
Fueglistaler S, Dessler A E, Dunkerton T J, Folkins I, Fu Q and Mote P W 2009 *Rev. Geophys.* **47** RG1004
Govindasamy B and Caldeira K 2000 *Geophys. Res. Lett.* **27** 2141–4
Govindasamy B, Caldeira K and Duffy P 2003 *Glob. Planet. Change* **37** 157–68
Govindasamy B, Thompson S, Duffy P, Caldeira K and Delire C 2002 *Geophys. Res. Lett.* **29** 2061
Guo S, Bluth G J S, Rose W I, Watson I M and Prata A J 2004 *Geochem. Geophys. Geosyst.* **5** Q04001
Hansen J, Sato M, Ruedy R, Lo K, Lea D W and Medina-Elizade M 2006 *Proc. Natl Acad. Sci. USA* **103** 14288–93
Hegerl G C *et al* 2007 *Climate Change 2007: The Physical Science Basis. Contribution of Working Group I to the Fourth Assessment Report of the Intergovernmental Panel on Climate Change* ed S Solomon, D Qin, M Manning, Z Chen, M Marquis, K B Averyt, M Tignor and H L Miller (Cambridge: Cambridge University Press)
Hofmann D J and Oltmans S J 1993 *J. Geophys. Res. Atmos.* **98** 18555–61
Keith D 2000 *Annu. Rev. Energy Environ.* **25** 245–84
Lacis A A and Mishchenko M I 1995 *Aerosol Forcing of Climate* ed R J Charlson and J Heinztenberg (Chichester: Wiley) pp 11–42
Manzini E and McFarlane N A 1998 *J. Geophys. Res. Atmos.* **103** 31523–39
Matthews H D and Caldeira K 2007 *Proc. Natl Acad. Sci. USA* **104** 9949–54
McCormick M P, Thomason L W and Trepte C R 1995 *Nature* **373** 399–404
McPeters R D 1993 *Geophys. Res. Lett.* **20** 1971–4
Meehl G *et al* 2007 *Climate Change 2007: The Physical Science Basis. Contribution of Working Group I to the Fourth Assessment Report of the Intergovernmental Panel on Climate Change* ed S Solomon, D Qin, M Manning, Z Chen, M Marquis, K B Averyt, M Tignor and H L Miller (Cambridge: Cambridge University Press)
Morcrette J J 1991 *J. Geophys. Res.* **96** 9121–32
Rasch P J, Tilmes S, Turco R P, Robock A, Oman L, Chen C C, Stenchikov G L and Garcia R R 2008a *Phil. Trans. R. Soc.* A **366** 4007–37
Rasch P J, Crutzen P J and Coleman D B 2008b *Geophys. Res. Lett.* **35** L02809
Rayner N A, Parker D E, Horton E B, Folland C K, Alexander L V, Rowell D P, Kent E C and Kaplan A 2003 *J. Geophys. Res.* **108** 4407
Read W G, Froidevaux L and Waters J W 1993 *Geophys. Res. Lett.* **20** 1299–302
Robock A, Oman L and Stenchikov G L 2008 *J. Geophys. Res.* **113** D16101
Rosen J M, Kjome N T, Fast H, Khattatov V U and Rudakov V V 1992 *Geophys. Res. Lett.* **19** 1751–4
Rozanov E, Schlesinger E M and Zubov V A 2001 *Geophys. Res. Lett.* **106** 27233–54
Sander S P *et al* 2000 *JPL Publication 00-3*
Schraner M *et al* 2008 *Atmos. Chem. Phys.* **8** 5957–74
Solomon S 1999 *Rev. Geophys.* **37** 275–316
Solomon S *et al* 2007 *Climate Change 2007: The Physical Science Basis. Contribution of Working Group I to the Fourth Assessment Report of the Intergovernmental Panel on Climate Change* ed S Solomon, D Qin, M Manning, Z Chen, M Marquis, K B Averyt, M Tignor and H L Miller (Cambridge: Cambridge University Press)
SPARC 2006 Assessment of stratospheric aerosol properties (ASAP) *SPARC Report No. 4, WCRP-124* WMO/TD No. 1295, ed L Thomason and T Peter
Steele H M and Hamill P 1983 *J. Atmos. Sci.* **12** 517–28
Stowe L L, Carey R M and Pellegrino P P 1992 *Geophys. Res. Lett.* **19** 159–62
Teller E, Wood L and Hyde R 1997 Globalwarming and ice ages: 1. Prospects for physics basedmodulation of global change *UCRL-JC-128157* Livermore National Laboratory, Livermore, CA
The Royal Society 2009 *Geoengineering the Climate: Science, Governance and Uncertainty Report* ISBN 978-0-85403-773-5
Thomason L W 1992 *Geophys. Res. Lett.* **19** 2179–82
Tilmes S, Garcia R R, Kinnison D E, Gettelman A and Rasch P 2009 *J. Geophys. Res. Atmos.* **114** D12305
Tilmes S, Muller R and Salawitch R 2008 *Science* **320** 1201–4
von Kuhlmann R, Lawrence M G, Crutzen P J and Rasch P J 2003 *J. Geophys. Res.* **108** 4729
Weisenstein D K, Ko M K W, Dyominov I G, Pitari G, Ricciardulli L, Visconti G and Bekki S 1998 *J. Geophys. Res. Atmos.* **103** 1527–47
Weisenstein D K, Penner J E, Herzog M and Liu X 2007 *Atmos. Chem. Phys.* **7** 2339–55
Weisenstein D K, Yue G K, Ko M K W, Sze N D, Rodriguez J M and Scott C J 1997 *J. Geophys. Res. Atmos.* **102** 13019–35
Winker D and Osborn M 1992 *Geophys. Res. Lett.* **19** 167–70
WMO 2007 Scientific assessment of ozone depletion: 2006 *Global Ozone Research and Monitoring Project-Report No. 50* Geneva, Switzerland, p 572